Fully Embedded Ultra-Wideband Multilayer Balun into Organic Packaging Substrate

Fully Embedded Ultra-Wideband Multilayer Balun into Organic Packaging Substrate

Khaled Aliqab*, Jiasheng Hong

Department of Electrical, Electronic and Computer Engineering, School of Engineering and Physical Sciences, Heriot-Watt University, Edinburgh, EH14 4AS, UK
*kma20@hw.ac.uk

Abstract: This paper presents a novel miniaturised ultra-wideband (UWB) multilayer balun embedded into organic packaging substrate of liquid crystal polymer (LCP). The broadside coupled stripline structure is adopted in this work to realise ultra-wideband performance and TEM mode. The fabricated prototype is self-packaged for EM shielding, and lightweight, with a small footprint. The proposed balun design achieves excellent amplitude and phase balances within the entire bandwidth, centred at 6.2 GHz. Simulation and measurement results show very good agreement.

1. Introduction

In RF front-end passive devices, baluns constitute a key component in balanced circuit topologies including push-pull amplifiers [1]. The balun performs balanced-to-unbalanced signal transformation, which is one of its functions, for instance in connecting balanced antennas to unbalanced transmission lines [2]. The demand for noise reduction, for example in analogue circuits, is increasing. That can be accomplished using balanced input/output lines. That essentially means forming two conductors with equal potential but opposite phases (180° phase difference), for example twisted-pair cables.

In recent years, UWB-based systems have received increasing attention as a result of the features associated with these systems. High channel capacity, low consumption in transmission power and a great immunity to multipath interferences are all examples of that. In the meantime, there is an increasing demand for packaging UWB devices for system integration [3]-[4].

Balun designs and configurations vary considerably. However, most of the reported baluns are either narrowband or with a fractional bandwidth (FBW) smaller than 100% [5]-[7], and only few UWB baluns with FBW > 100% have been reported [8]-[10]; none of them are packaged. It is more challenging to design and realize packaged UBW balun with good performance such as amplitude and phase balances over an ultra-wide operation frequency band.

This paper's main objective is to present, at the first time, a new, inexpensive, self-packaged balun design with an ultra-wideband bandwidth, compact size and high performance, with full (EM) shielding. The balun is self-packaged due to the fact that the top and bottom layers are the conductor ground for the embedded transmission line circuit elements and coplanar waveguide ports are used to directly excite the balun. Such a small, lightweight packaged balun is desirable in a highly integrated system to minimise unwanted cross-talking, as well as to accommodate the system's restraints in terms of size and weight. Low-cost multilayer liquid crystal polymer technology is deployed in this work for the physical implementation. LCP multilayer technology provides an effective solution for the low-cost and high-performance interconnect and packaging of microwave systems.

2. Balun design and analysis

Fig.1(a) illustrates the proposed design schematic, consisting of Z_a the port impedance (typically 50 ohms), two quarter-wavelength coupled-line sections with even and odd impedances Z_{oe} Z_{oo} respectively, and finally Z_b, which is the output impedance of the coupled-line sections. Referring to the ports assignment shown in Fig. 1(a), the S-parameters of the Marchand balun [11] are ideally defined as:

$$S_{11} = 0; S_{21} = -S_{31} \quad (1)$$

The relationship characterising Z_{oe} and Z_{oo} for various Z_a and Z_b sets is [12]:

$$Z_{oe} = \frac{1}{\frac{1}{Z_{oo}} - \sqrt{\frac{2}{Z_a Z_b}}}; Z_{oo} = \frac{1}{\sqrt{\frac{2}{Z_a Z_b}} + \frac{1}{Z_{oe}}} \quad (2)$$

For the Z_b effect on the matching bandwidth response to be observed (Z_a=50 and Z_{oo} were fixed at 31 ohms), four different values of Z_b= 50, 60, 70 and 80 ohms were tested for comparison, corresponding to Z_{oe}= 251.6, 155, 119 and 101 ohms respectively, as illustrated in Fig. 1(b). As shown in Fig. 1(b), Z_b=50 ohms provides a single transmission-pole passband response, as indicated by S_{11}, while Z_b =60 ohms results in two transmission poles similar to the Chebyshev response in the passband with a sensible, e.g. 20 dB matching bandwidth. Further increasing Z_b degrades the matching bandwidth. Therefore, the value of Z_b=60 ohms was specifically chosen for this design.

The corresponding design graph is shown in Fig. 1(c). This clearly defines the relationship between Z_{oe} and Z_{oo} as a rational, advantageous behaviour when compared with a linear characteristic as a result of using a microstrip quasi-TEM structure. The nature of the relationship between Z_{oe} and Z_{oo} is mainly influenced by the structure used, namely the broadside-coupled stripline, supporting TEM propagation and providing a rational relationship, whereas the coupled microstrip quasi-TEM lines support a linear

relationship. This rational behaviour favours a linear structure, because it shows a marked difference between Z_{oe} and Z_{oo} impedance values, resulting in strong coupling that is essential for a UWB design. On the other hand, non-TEM or quasi-TEM coupled line structures can affect the wideband response considerably due to unequal phase velocity of the odd and even modes.

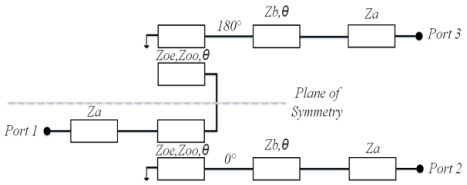

a

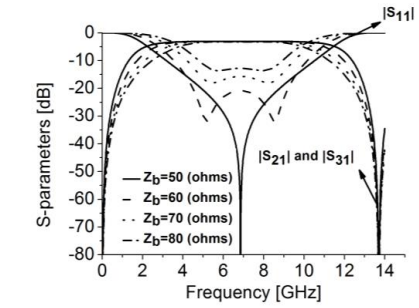

b

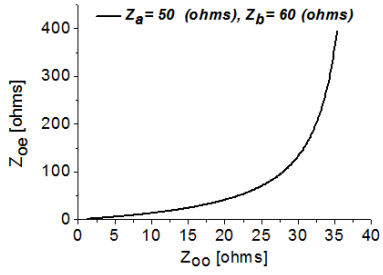

c

Fig. 1. *Proposed design*
(a) *Circuit model,* **(b)** *Simulated frequency response of the design,* **(c)** *Relationship between Z_{oe} and Z_{oo} for Z_b=60 ohms*

For a given set of Z_a and Z_b, the coupled-line parameters (Z_{oe} Z_{oo}) can vary, resulting in various fractional bandwidths. Nevertheless, any of the (Z_{oe} Z_{oo}) combinations located on the line in Fig.1(c) will result in Z_b=60 ohms.
In order to have UWB performance, the coupling factor related to the coupled lines has to be large, which means a high impedance ratio between (Z_{oe} Z_{oo}) requiring tight coupling gaps. In addition, it is critical to have the same phase velocity of the odd and even modes for the tightly coupled line. However, that is not easily achieved with edge-coupled, quasi-TEM transmission line structures, which most of the previous studies have tended to use. As a result, a broadside TEM coupling structure is implemented here instead.

As can be seen in Fig.1(c), multiple (Z_{oe} Z_{oo}) combinations are shown on the 60 ohms output line. However, some of these are inapplicable, extremely difficult to obtain or simply inappropriate as far as performance and physical implementation are concerned. The two main factors controlling the (Z_{oe} Z_{oo}) values in a stripline configuration are the width and vertical gap spacing of the two coupled lines. By fixing the vertical gap spacing between the two lines to a 100 micro meter and tuning the width, it was found that 0.3 mm provides the desired (Z_{oe} Z_{oo}) combination corresponding to (Z_{oe}=155, Z_{oo}=31 ohms). Also, this line width provides good fabrication tolerance to overcome any issues in the manufacturing process. Thus, the idea of using LCP bonded PCB multilayer technology is proposed in here to accomplish the required vertical tight coupling and the very thin 100 micro meters distance.

The design is stripline-based, in which the whole layout is enclosed within a self-designed package, in which the package is an integral part of the hosted design fabrication process. Fig.2 shows the 3D view, along with the proposed design's layer stack. As can be seen in Fig. 2(a), Layer (1) presents the interface of the enclosed design to the outer system and the first ground plane for the enclosed stripline layout. It contains the input and output feeding lines designed to match 50-ohm impedance in a coplanar waveguide (CPW) structure, in which the signal line and ground are located at the same level, separated by a small gap. These feeding lines are connected to the hosted board with the help of via holes. In addition, these are also used for grounding, as shown in Layer (3) with reference to the proposed design topology in Fig. 1(a). Layers (2) and (3) contain the layout of the proposed balun where broadside coupling is clearly illustrated between the two quarter wavelength coupled-line sections. These are etched on the same substrate with a thickness of a 100 micro meter to provide the required high coupling factor. Layer (4) is completely metalised, which is the ground plane of the grounded coplanar waveguide structure (G-CPW), and the second ground plane for the enclosed stripline layout.

When the signal is transmitted through the single-ended 50- ohm input feed line (unbalanced) from CPW to stripline level, it is simultaneously coupled to the lower quarter-wavelength lines located at Layer (3) with the same magnitude, but with a 180° phase shift. This differential signal is then transmitted from stripline level back up to CPW level through via holes which provide the balanced signal output.

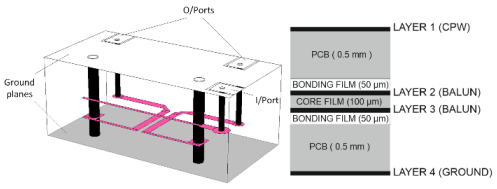

a *b*

Fig. 2. Multilayer balun
(a) *3D model of the proposed multilayer balun,* ***(b)*** *Cross-section view of the layer stack implemented*

The investigations were carried out using two different substrates, as shown in Fig. 2(b). The printed circuit board (PCB) layers located at Layers (1) and (4) used Rogers RO3003 substrate with a dielectric constant of 3.0, loss tangent of 0.0025 and a thickness of 0.5 mm. In Layers (2) and (3), an LCP film (core and bonding films) had the same dielectric constant and loss tangent as the PCB, but with a thickness of 100 micro meter. The PCB and LCP were bonded together without any other adhesives using an LCP bonding film with almost the same characteristics as the LCP core film, but with a thickness of 50 micro meter. A multilayer lamination process was developed to implement the designed prototype. As previously mentioned, the metal tracks were etched on the LCP core film, which had a melting temperature of 315°C, which is different to the LCP bonding film's melting temperature of 280°C.

Fig. 3 illustrates each of the individual design layers, along with the dimensions used during the prototype fabrication. Final dimensions are as follows: L1 =2.7, W1=1.8, W2=2.2, g1=0.2, L2=1.4, W3=0.8, L3=13.1, W4=0.3, L4=6.3, g2=0.5, W5=0.7, L5=5.2, W6=0.8, L6=5, width=20 and length=10 (all in millimetres). Via holes for input and output feeding lines are 0.5mm in diameter, while the grounding via holes are all 1.0mm in diameter.

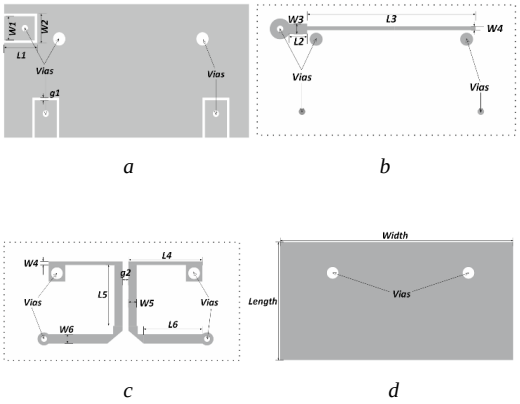

a *b*

c *d*

Fig. 3. *Balun layers' dimensions*
(a) *Layer1,* **(b)** *Layer2,* **(c)** *Layer3,* **(d)** *Layer4.*

3. Lamination and fabrication optimisation

One of the most critical aspects of a multilayer design is providing the vertical transition between different layers. That is typically achieved by using via holes. As a result, multiple lamination cycles are needed, in which an inner layer connection is established first, and then the whole layer stack is laminated together. Sometimes, that requires more than two iterations of lamination cycles to bond all the layers together.

Most of the previously reported work has typically used at least two multiple lamination iterations where there are inner connections between different layers. However, that is extremely time-consuming, and increases the margin of error while also affecting bonding quality, vertical transitions, output performance and various other factors. Therefore, an optimised procedure was developed which needed just one lamination cycle for the whole prototype fabrication.

There are two types of via holes related to this design, namely through via holes which extend from the top to the bottom layer, and blind via holes which originate from either the top or the bottom layer and terminate at one of the inner layers, as shown in Fig. (4):

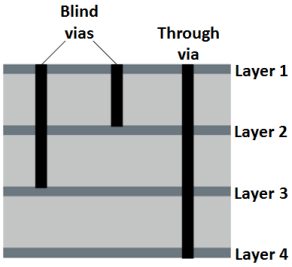

Fig. 4. *Proposed design via hole classification*

Each one of these via holes type is realised in a different way. Firstly, regardless of the number of layers and inner connections, all layers are bonded together. After that, each type, namely blind and through via holes, is realised following a different procedure.

3.1. Blind Via Holes

In the CPW interface located in Layer 1, all the I/O feeding lines have some copper etched out in the form of a circle at the end of the line, as illustrated in Fig. 3(a). Using the CO2 laser drilling machine, the laser is concentrated on these circles, in which it would burn out the dielectric material, only stopping at the copper patch underneath these circles in the stripline layer located in Layers 2 and 3, which it cannot penetrate. Next, these via holes are filled with silver paste to obtain a strong connection. This methodology was used for the input and output feeding lines connection.

3.2. Through Via Holes

This type of via hole is used here to provide the grounding via holes connection. Having a strong ground connection is a critical issue, especially if inner layers of the design need to be connected to the ground plane. Typically, most reported work has tended to use direct drilling from top to bottom, and if inner layers need to be connected, the via hole is drilled where the connection to the ground plane is needed. However, that provided poor connections to ground, since the connection is only established around the edges of the circle-shaped via hole. In some cases, that connection could even be lost as a result of multiple laminations or through not having a perfect alignment between layers. In fact, even if both the lamination and alignment were perfect, the connection would still be weak. Thus, an optimised procedure was developed to overcome these issues and offer a much better ground connection and, consequently, enhanced results.

In the same way as with the blind via holes, the copper was etched out in circle form in the CPW interface located in Layer 1, and the ground plane located in Layer 4, as shown in Figures3 (a) and (d) respectively. Firstly, a via hole was drilled from top to bottom using the drill machine, with a diameter of 0.5mm smaller than the etched-out circles at 1.0mm, as displayed in Figures 5(a) and (b). Secondly, again using the laser drill machine, the laser was

concentrated on the etched-out circles, and consequently burnt the dielectric out, only stopping at the copper patch in Layer 3, which it could not penetrate, where the connection to ground is needed. That resulted in having two types of via holes, the first one extending from top to bottom with a diameter of 0.5mm, the second with a diameter of 1.0mm extended from top to bottom and terminated at the circular patch located in Layer 3, as shown in Fig. 5. Finally, a silver paste was applied to fill up the via hole gaps and provide a solid ground connection.

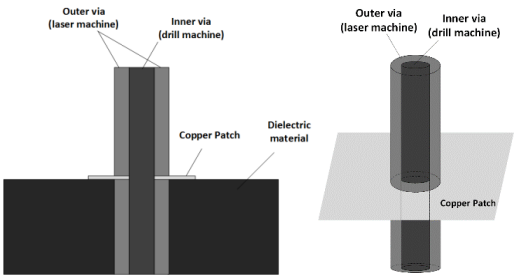

a *b*

Fig. 5. Proposed via implementation
(a) *Cross-section view*, ***(b)*** *3D view*

4. Implementation and experiment

Based on the above discussion, an UWB multilayer balun operating at 6.2 GHz with a fractional bandwidth (FBW) >100% was designed, simulated and fabricated. The balun was fabricated in-house and an N5225A PNA Microwave Network Analyser was used to obtain the final measured results. Fig. 6 shows the simulated and measured responses of the balun, including S-parameters as well as phase and amplitude balances. It has an ultra-wide operating bandwidth from 2.7 to 9.6 GHz, or a FBW of 111% at the centre frequency of 6.2 GHz. The simulated return loss is greater than 14 dB, with an insertion loss of 0.35 dB clearly shown in Fig. 6 (a). The amplitude and phase balances are illustrated in Fig.6 (b), in which the amplitude balance achieves ±0.37 dB, whereas a phase difference of ± 1.8° is achieved within the bandwidth provided. The measured insertion loss is better than 1.0 dB clearly shown in Fig. 6(a). The measured amplitude and phase balances are better than ±0.6 dB and ±2.8° respectively as illustrated in Fig. 6(b).

As can easily be seen from the graphs, the measurement results generally agree with the simulations, with the few variations attributed to fabrication tolerances. These variations were mainly caused by fabrication tolerances and by attaching the SMA's connectors to the circuit board where three of them were used. Each time one of them was soldered to the circuit board, it introduced a major temperature rise, causing the board to expand vertically. That results in the gaps between the coupled-line sections varying vertically, and thus the coupling also changes. Another reason for the discrepancies between the simulated and measured results is cutting the edges of the substrate. That resulted in different physical lengths between output ports 2 and 3. As a result, some phase variations can be seen between the simulated and measured results.

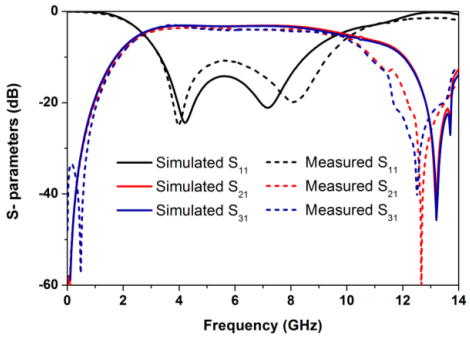

a

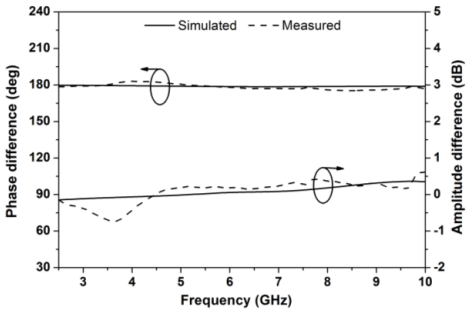

b

Fig. 6. Balun responses
(a) *Simulated and measured s-parameters*, ***(b)*** *Simulated and measured amplitude and phase balances*

The photographs of the fabricated balun prototype are displayed in Fig. 7, showing both sides of the design.

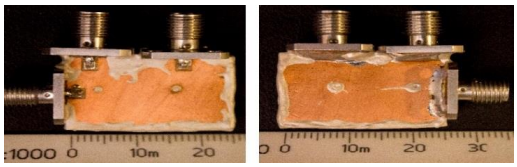

a *b*

Fig. 7. Photographs of the fabricated balun
(a) *Upper side*, ***(b)*** *Lower side*

A table with detailed performance comparison with related UWB balun designs from the literature is shown in Table 1. It includes the centre frequency f_0, the fractional bandwidth FBW, the insertion loss IL, the amplitude imbalance AB and finally the phase imbalance PB. Note that the results from [8] and [9] are based on simulated ones as the measured ones are not available. In Table 1, the balun depicted in Fig. 6 illustrates an outstanding measured amplitude and phase balances of 0.6 dB and 2.8° respectively extending throughout the whole UWB bandwidth centred at 6.2 GHz.

Finally, let us highlight the differences to other reported works and the advantages associated with the proposed design. It demonstrates a high-operating centre frequency with UBW bandwidth maintain outstanding AB and PB performances. That clearly illustrates the novelty, capability and significance of the proposed design. The proposed balun is a multilayer design based with a relatively small footprint adding on to the advantages related to this implementation. It is worth mentioning that to the best of our knowledge no such balun reported in the literature is electromagnetic (EM)-shielded with self-packaging feature. Therefore, the work introduced in this paper distinctively combines all the aforementioned advantages and thus it outstands.

Table 1 Performance comparison with other UWB baluns with FBW>100%

Ref.	Self-packaged with EM-shielding	f_o (GHz)	FBW	IL (dB)	AB (dB)	PB (deg)
[8] (Simulated)	No	7	114%	0.5	---	5
[9] (Simulated)	No	7.2	105%	0.4	0.5	10
[10] (Measured)	No	5	161%	2.3	1.5	12
This work (Measured)	**Yes**	**6.2**	**111%**	**1.0**	**0.6**	**2.8**

IL: insertion loss; AB: amplitude imbalance; PB: phase imbalance.

5. Conclusion

This paper presents a novel miniaturised multilayer balun using LCP technology. It demonstrates UWB performance using the broadside coupling structure. It shows that the design is self-packaged, with full EM shielding, and is light weight with a small footprint, reducing overall cost. It is a broadside-coupled, stripline-based design supporting TEM propagation and offering the best solution for UWB designs and for all aforementioned issues related to common- mode rejection.

Simulated and measured results demonstrate the proposed design's outstanding capability and significance, and these are in a good agreement, further validating the proposed design.

6. Acknowledgments

This work was supported by Al-Jouf University, Saudi Arabia. Khaled Aliqab would also like to thank all the staff in the electronic workshop at Heriot-Watt University for all their efforts in helping with this project.

7. References

[1] Hsu, P.-C, Nguyen, C., Kintis, M.: 'Uniplanar broad-band push–pull FET amplifiers', IEEE Trans. Microwave Theory Tech., 1997, 45, pp. 2150–2152
[2] Zhang, G., Wang, J., Wu, W.: 'Wideband balun bandpass filter explored for a balanced dipole antenna with high selectivity', Electron. Lett., 2016, 52, (13), pp. 1153–1155
[3] Han, L., Wu, K., Zhang, X.: 'Development of Packaged Ultra-Wideband Bandpass Filters', IEEE Trans. Microw. Theory Tech., 2010, 58, (1), pp. 220-228
[4] Cervera, F., Hong, J., Thomson, N.: 'Development of Packaged UWB Passive Devices Using LCP Multilayer Circuit Technology', Proceedings of the 7th European Microwave Integrated Circuits Conference, 2012, pp. 770-773
[5] Jiang, W.-B., Jin, L., Hu, J.-G., Yang, S.-Z.: 'Design of a miniaturized balun using low temperature co-fired ceramic technology', IEEE Electrical Design of Advanced Packaging & System Symposium (EDAPS), 2010, pp. 1-4
[6] Wu, P., Wang, Z., Zhang, Y.: 'Wideband planar balun using microstrip to CPW and microstrip to CPS transitions', Electron. Lett., Nov 2010, 46, (24), pp. 1611-1613
[7] Geng, Y., Wang, W., Chen, X., Han, L., Li, L., Zhang, W.: 'The Study and Design of a Miniaturized Microstrip Balun With a Wider Bandwidth', IEEE Antennas and wireless Propag. Lett., 2016, 15, pp. 1727-1730
[8] Nguyen, P. T., Abbosh, A., Crozier, S.: 'Ultra-Wideband Balun Using Microstrip to Slotline Transitions', IEEE Asia-Pacific Conference on Antennas and Propagation., Aug 2012, pp. 309-310
[9] Abbosh, A.: 'Planar ultra-wideband balun using coupled microstrip lines', Electron. Lett., 2013, 49, (10), pp. 662–664
[10] Wu, Y., Yao, L., Jiao, L., Wang, W., Liu, Y.: 'UWB balun with complete ground based on vertically mounted planar structure', Electronics Lett., Mar 2016, 52, pp. 405-406
[11] Marchand, N.: 'Transmission line conversion transformers', Electronics, 1942, 17, (12), pp. 142-145
[12] Ang, K. S., Robertson, I. D.: 'Analysis and design of impedance transforming planar Marchand baluns', IEEE Trans. Microw. Theory Tech., Feb 2011, 49, (2), pp. 402–406